Modelling and Design for Position-Free Inductive Couplers with the Homogeneous-Flux Transmitting Coil in Wireless Power Transfer Systems

Yi Dou, Student Member, IEEE, Xiaosheng Huang, Member, IEEE, Ziwei Ouyang, Senior Member, IEEE, and Michael A.E. Andersen, Member, IEEE

Abstract—This paper presents a design algorithm to combine the analytical magnetic flux modelling and the genetic algorithm (GA) for position-free inductive couplers in inductive power transfer (IPT) systems. The design concept can enhance the position tolerance significantly by making the transmitting coil generate a homogeneous flux density at the target receiving position. Based on the analytical magnetic flux models and the proposed design algorithm, the winding configurations for the air-core transmitting coils or magnetic shielded transmitter coils can be directly generated. Two case studies demonstrate the design algorithm: the analytical magnetic flux models and the generated homogeneous flux density are verified by 2D FEM simulation and measurement results. Furthermore, the non-interference for the inverters'/rectifiers' operation with the position shift is experimentally verified on the 6.78 MHz prototypes.

Index Terms—Inductive power transfer, genetic algorithm, position-free function, coil design.

I. Introduction

Inductive power transfer is an emerging and fast-developing technology that can significantly enhance the power transfer convenience and reduce manual labour during the devices' charging process. In the last few years, the applications of the IPT came up with battery charging for low-power consumer electronics [1] and high-power electrical vehicles [2,3]. Besides, it is under much expectation for extended applications in implanted medical devices and autonomous systems [4]–[9].

High position tolerance is always a preferable feature for IPT systems where the couplers may occasionally meet misalignment issues between the transmitter and the receiver coils. The wireless charging systems for inspection drones are a typical application. The position tolerance for the couplers needs further enhancement due to the requirement for higher system reliability and a reduced maintenance cost. Under this circumstance, the mechanical structure which adapts to the receiver movement or the multi-coil transmitter solution cannot address the challenge for the applications. Thus, novel solutions for position-free couplers are required [10].

In brief, the operation shift from the misalignment issue in an IPT system comes from the induced magnetic coupling shift. As illustrated in Fig.1, the circuit model of the coupled coil is depicted in a T-type model, where

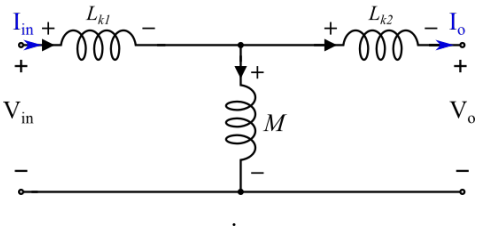

Fig. 1. The T-type circuit model for the inductive coupler: M represents the mutual inductance formed by the transmitting and the receiving coil and L_{k1}/L_{k2} represent the leakage inductance on the transmitting/receiving side correspondingly

Table I
Overview of the voltage/current gain for commonly used compensation in IPT

Compensation type	Voltage/ Current Gain
Series-series	$\frac{I_o}{I_{in}} = \frac{1}{\omega M}$
Series-parallel	$\frac{V_o}{V_{in}} = \frac{(L_{k2}+M)}{M}$
Parallel-series	$\frac{V_o}{V_{in}} = \frac{M}{(L_{k1}+M)}$
LCC-series	$\frac{V_o}{V_{in}} = \frac{M}{L_{series}}$

M represents the mutual inductance between the coupled coils and L_{k1}/L_{k2} are the leakage inductance on the transmitting/receiving side correspondingly. Once the relative position between the transmitting and the receiving coils shifts, the mutual inductance and the leakage inductance will also shift. Table I reviewed several commonly used compensation in the inductive power transfer and their voltage/current gain. The expressions in the table indicate that the position shift for the coils impacts the operation of the IPT systems. Besides, an efficiency reduction results typically from the misalignment issue as well [11,12].

To counter the mutual inductance shift induced by the misalignment, people naturally proposed to design the coupler whose mutual inductance is independent of the relative position. The definition of mutual inductance is given in equation I

$$M = \frac{\lambda_r}{i_t} = \frac{\sum \phi_n}{i_t} = \frac{\sum (\iint_s B)_n}{i_t} \tag{1}$$

, where λ_r is the flux linkage on the receiving coil, which also equals to the total magnetic flux received $\sum \phi_n$ or the total surface integral of the magnetic flux density received $(\iint_s B)_n$; the i_t is the excitation current on the transmitting coil generating the flux. It is found that once the generated flux can be regulated as homogeneous, the position-free feature of the coupler is then achieved.

The homogeneous-flux transmitter coil was initially reported in [13], where the auxiliary windings compensate the in-homogeneous flux generated by the coil with equal pitches. However, the literature [13] does not cover the coil modeling or design guideline to implement the solution to generalize the coil design. Afterward, an design process for the transmitter coil is presented in [14]. The design method in [14] can be summarized as: firstly, the continues current distribution to generate a homogeneour flux desity is directly solved. Then, the transmitter coils will be designed to fit the continuous current distribution by several discrete turns of windings. However, the current distribution solving was not presented in the literature but still relies on the finite-element-analysis simulation. Besides, the current fitting process will also induce system error.

Genetic algorithm (GA) is an alternative to searching solutions with specific optimization targets, which was initially presented in [15]. Particularly in this investigation, to design a position-free transmitter coil with the homogeneous flux generated, the winding configuration can be directly generated by applying the GA based design algorithm. The concept has been technically demonstrated in [16], nevertheless, the detailed design process and analysis were not covered.

With the help of magnetic material to shield and regulate the magnetic flux, the transmitting coil in the IPT system can obtain better magnetic coupling and EMI performance. Nevertheless, the modeling and design for the shielded coils are rarely reported. The difficulty to theoretically analyze the shielded coil is because the material from a homogeneous media breaks the distribution space of the electromagnetic field. Therefore, the analytical model is challenging to be solved. Previously, the designers usually relied on FEM simulation to lead the design, which is time-consuming and complicated to implement. Initiatialially, the design challenge is addressed by this investigation.

In this paper, the design algorithms for both the air-core and the shielded position-free transmitting coils are proposed, analyzed, and demostrated on IPT prototypes. By following the design results, the transmitter coils are able to generate the homogeneous magnetic flux at the target position to counter the operation shifting from the receivers' movement. In section II, we present the magnetic flux modelling for the air-core and shielded transmitter coil, which works as the fundamental analytical model for the proposed design algorithm. In section III, the modified GA-based design algorithm is introduced with detailed design considerations and analysis. In section IV, two case studies are presented, one for the normalized air-core transmitter coil design and the other for the shielded transmitter coil design. Next, the simulation and experimental results are provided to verify the proposed design algorithm. Finally, section V concludes the paper.

II. Magnetic Flux Modelling of the transmitting Coils in Inductive Power Transfer Systems

In this section, the magnetic flux density generated by the transmitter coil in a disc shape is modeled both for air-core transmitter coils and shielded transmitter coils. In Fig.2, an illustration in half-piece of the coil is shown. The magnetic shield, which usually is a slice of magnetic material, is attached under the windings in the figure. The flux-density modelling originally refers to the Biot-Savart law, which reveals the magnetic flux density of the testing point produced by a filamentary current source [17]. In the shielded coils‘ modelling of shielded coils, the current-mirror method is modified by adding several virtual currents to the original source current as in the free-space environment, which can be found in [18,19] with the similar concept. With the flux-density modelling, the inductance modelling for the coupler can also be obtained.

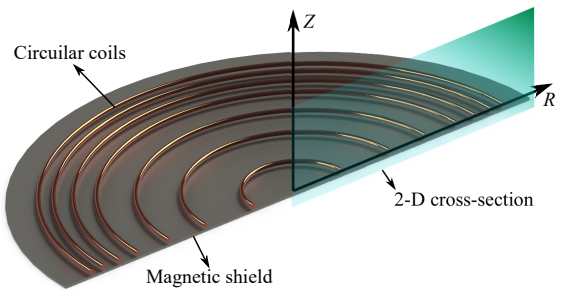

Fig. 2. 3D illustration of the shielded transmitting coils in the inductive coupler in half-piece and the 2-D cross section marked as the reference for the simplification during modelling.

A. Flux-Density Modelling for Air-Core transmitting Coils

In typical IPT systems, the power transmission distance is much larger than the wires' diameters, and each winding is connected in series to enhance the flux density generated. Hereby, the windings' configuration can be simplified when modeling the coils in the disc shape: The current generating flux on the windings is simplified as filamentary current, which locates at the center of the round wires. Besides, and the connection part and the terminals of the components are neglected.

The flux-density model is built in the magneto-static field considering the operation frequency of the systems is

normally limited as below several tens of mega-hertz. The Biot-Savart law, which initially is experimentally found, reflects the magnetic flux density produced as

$$d\vec{\mathrm{B}} = \frac{\mu_0}{4\pi}\frac{I d\vec{\ell} \times \vec{\mathrm{a}_R}}{R^2} \tag{2}$$

, where $d\vec{\mathrm{B}}$ is the produced magnetic flux density; $d\vec{\ell}$ is the length of the filamentary current source; I is the current carried by the element current source; $\vec{\mathrm{a}_R}$ is the unit vector pointing from the filamentary current source to the target point; and R is the norm (the distance) of the vector from the filamentary current source to the target point. Based on the Biot-Savart law, the magnetic flux density generated by a line current source can be calculated by

$$\vec{\mathrm{B}} = \frac{\mu_0}{4\pi}\int_c \frac{I d\vec{\ell} \times \vec{R}}{R^3} \tag{3}$$

, where $\vec{R}$ represents the vector from the each element current source to the target point and R represents the norm of the each vector correspondingly.

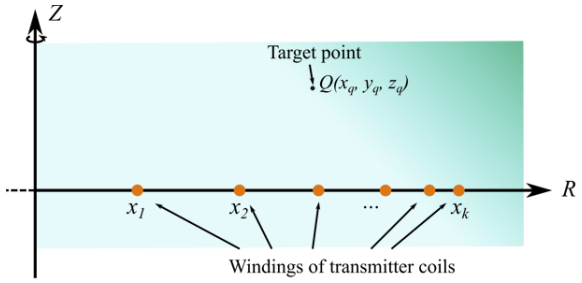

Fig. 3. Cross-section illustration of the air-core transmitting coils in the inductive coupler: all the windings located on the R-axis to form a disc-shape coil, and the target points are marked as Q above the coil.

A 2-D illustration from the cross-section's view of the air-core coil model is illustrated in Fig.3: The several turns of the winding locate on the R-axis in the polar coordinate and the target point Q is the position where the generated magnetic flux density will be calculated. Correspondingly, the positions of each transmitting winding are denoted as x_1, x_2 ...x_k on the R-axis and the position of target point Q is denoted as (x_q, y_q, z_q). Then the flux-density at the target point can be derived as

$$\vec{\mathrm{B}_Q} = \sum_{i=1}^{k}\int_{\theta=0}^{2\pi} \frac{\vec{I_s}(\theta) \times \vec{R_o}(x_q, y_q, z_q, x_k, \theta)}{R_o^3(x_q, y_q, z_q, x_k, \theta)} \tag{4}$$

, where $\vec{I_s}(\theta)$ is the element current source; $\vec{R_o}$ is the distance vector and R_o is the norm of this distance vector, which can be calculated as

$$\vec{I_s} = \begin{bmatrix} -sin(\theta) \\ cos(\theta) \\ 0 \end{bmatrix}, \vec{R_o} = \begin{bmatrix} x_q \\ y_q \\ z_q \end{bmatrix} - x_k \cdot \begin{bmatrix} cos(\theta) \\ sin(\theta) \\ 0 \end{bmatrix} \tag{5}$$

By following (4), the magnetic flux density generated by the winding can be calculated. For the other winding configuration, the magnetic flux can also be calculated by implementing equation (3) by adapting the winding's shape correspondingly.

B. Flux-Density Modelling for Coils with Magnetic Shield

Transmitter coils with magnetic shielding have increasing requirements in industrial applications to fulfill the EMI requirement and enhance system stability. The structure of the shielded coils is similar to the planar/thin-film inductors. However, few investigations were reported regarding their mathematical modelling in inductive power transfer systems, even less regarding the magnetic flux modelling [20]–[22]. Therefore, in order to cover the shielded transmitter coils in the model, the current-mirror method is applied to model the flux density generated.

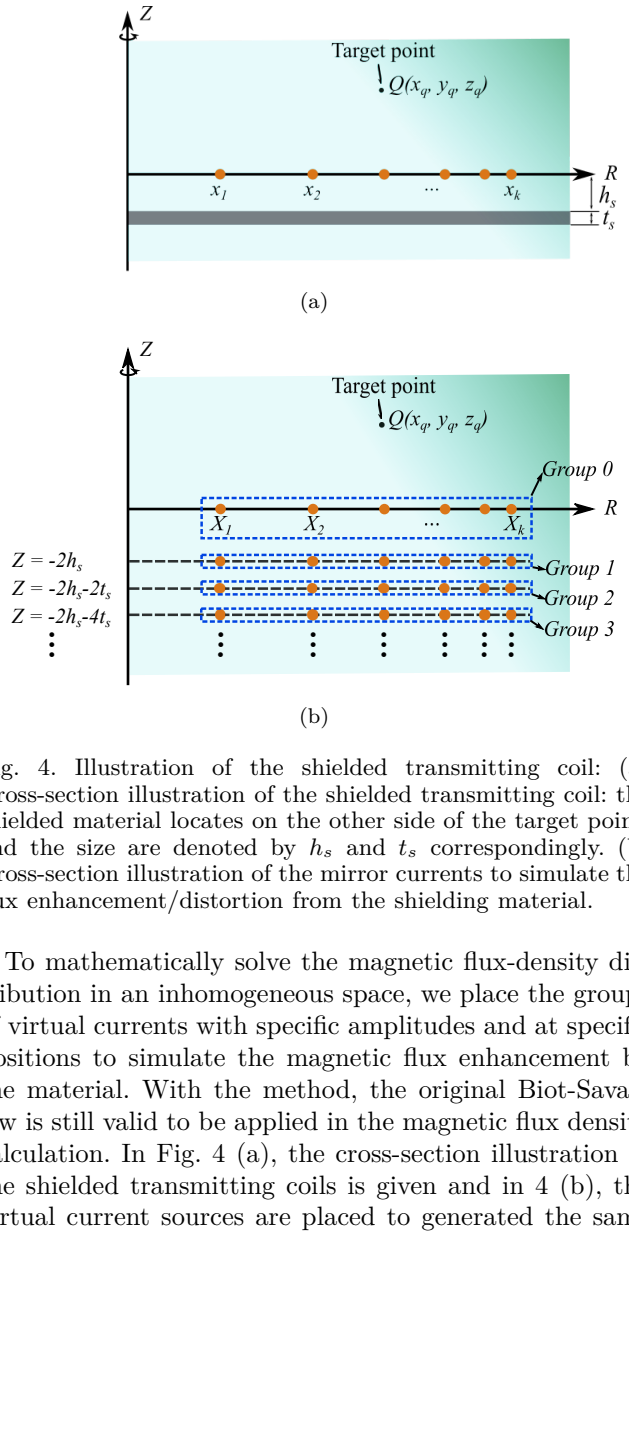

Fig. 4. Illustration of the shielded transmitting coil: (a) Cross-section illustration of the shielded transmitting coil: the shielded material locates on the other side of the target point, and the size are denoted by h_s and t_s correspondingly. (b) Cross-section illustration of the mirror currents to simulate the flux enhancement/distortion from the shielding material.

To mathematically solve the magnetic flux-density distribution in an inhomogeneous space, we place the groups of virtual currents with specific amplitudes and at specific positions to simulate the magnetic flux enhancement by the material. With the method, the original Biot-Savart law is still valid to be applied in the magnetic flux density calculation. In Fig. 4 (a), the cross-section illustration of the shielded transmitting coils is given and in 4 (b), the virtual current sources are placed to generated the same

magnetic flux as in (a), where the magnetic flux density at the target point can be solved. The magnetic flux density for the shielded coils $\vec{B_{qs}}$ can be calculated as

$$\vec{B_{qs}} = \vec{B_q} + \vec{B_{mir}} \tag{6}$$

, where $\vec{B_q}$ is the generated flux density from the coils as in the free-space, and $\vec{B_{mir}}$ is the generated flux density from the virtual current sources as

$$\vec{B_{mir}} = \sum_{n=0}^{\infty}\sum_{i=1}^{k}\int_{\theta=0}^{2\pi}\frac{\lambda_n \vec{I_s}(\theta)\times\vec{R_o}(x_q,y_q,z_q+2h_s+2(n-1)t_s,x_k,\theta)}{R_o^3(x_q,y_q,z_q+2h_s+2(n-1)t_s,x_k,\theta)} \tag{7}$$

, where λ_n is the correction coefficient for the amplitude of the current sources. The positions for the current sources are also modified as in the equations and the illustration. In the equations, the distance between the transmitting coil and the magnetic shielding, and the thickness of the shielding material are qualified as h_s and t_s correspondingly. The correction coefficient can be calculated by

$$\lambda_n = \begin{cases} \eta \quad ,if\ n=0 \\ (\eta^2-1)\eta^{2n-1} \quad ,if\ n>0, \eta=(\mu_r-1)/(\mu_r+1) \end{cases} \tag{8}$$

, where μ_r is the relative permeability of the shielding material. It is noticed that an infinite number of current sources should be placed to simulate the enhancement from the magnetic shielding. During the practical design, only a limited number of current source will be included for fair simplification. Therefore, by combining equation (6) to (8), the generated magnetic flux density can be calculated as a a function of the windings' configuration (as windings' position x_1, x_2...x_k) and the shielded material's configuration (including the distance h_s, the shielding material's thickness t_s and the permeability of the material μ_r).

C. Inductance Modelling for Inductive Couplers

The original definition of the inductance is

$$L = \frac{\lambda}{i} \tag{9}$$

, where λ is the flux linkage coupled by the windings, and i is the excitation current to generate the flux. To build the circuit model based on winding configurations, the inductance modelling should be derived for the afterward WPT system design. In Fig.5, an 2D illustration shows a pair of transmitting coil and receiving coil put in parallel. The distance between the coils is h_p, while the position of the receiving coil is denoted as $x_{r1}, x_{r2}...x_{kr}$. Correspondingly, the self-inductance of the transmitting coil can be calculated as

$$L_{self} = \sum_{i=1}^{k}\int_0^{2\pi}\int_0^{x_k}(\vec{B}(r\cdot cos\varphi, r\cdot sin\varphi, 0)\times\begin{bmatrix}0\\0\\1\end{bmatrix})\mathrm{d}\varphi\mathrm{d}r \tag{10}$$

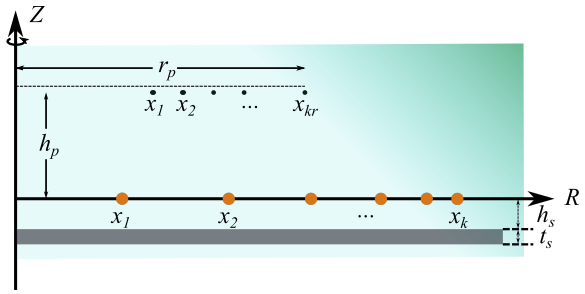

Fig. 5. Cross-section illustration of for self-/mutual-inductance for an inductive coupler.

, where only the vertical part of the flux density is included in the calculation and the $\vec{B}$ should be replaced by $\vec{B_q}$ or $\vec{B_{qs}}$ if considering a shielded coil. The mutual inductance between the coils can also be calculated as

$$M = \sum_{i=1}^{kr}\int_0^{2\pi}\int_0^{x_{kr}}(\vec{B}(r\cdot cos\varphi, r\cdot sin\varphi, h_p)\times\begin{bmatrix}0\\0\\1\end{bmatrix})\mathrm{d}\varphi\mathrm{d}r \tag{11}$$

, where h_p is the distance between the transmitting and the receiving coils. Similarly, only the vertical flux is included in the calculation for the paralleled transmitter and receiver coils. If the transmitter coil and receiver coil need to be in other spatial relations, the inductance can also be calculated by modifying the selected flux direction.

So far, the flux modelling and the inductance modelling applied for the following design have been built. The validation and the sensitivity of the models will be provided in the section IV based on FEM simulation and measurement results.

III. GA Based Winding Configuration Design Algorithm

In this section, the design algorithm is proposed to directly generate transmitting winding configurations to generate homogeneous flux density at the target receiving range to improve position tolerance significantly. Compared with the method in [14], solving the current distribution is unnecessary, which makes the proposed design method much intuitive and easily applicable. Generally, several optimization algorithms may serve as the method, such as the gradient descent method and the pattern search. Hereby we proposed a genetic algorithm (GA) based algorithm to achieve the design. Based on the discontinuity and the undefined monotone of the winding configuration, theoretically, the GA-based algorithm is able to find the global optimum as the solution In addition, it is convenient to define constraints in the GA-based algorithm to adapt the physical limitation for the practical transmitting coils. The fundamental of the genetic algorithm and its industry application can be initially found in [23].

GA simulates the natural evolution: after the iteration process, the most adaptable candidates will survive as the

optimized solution. An illustration of the proposed GA-based design algorithm is shown in Fig.6, and the iteration will operate in loop within selection and genetic operators until a termination condition is eligible.

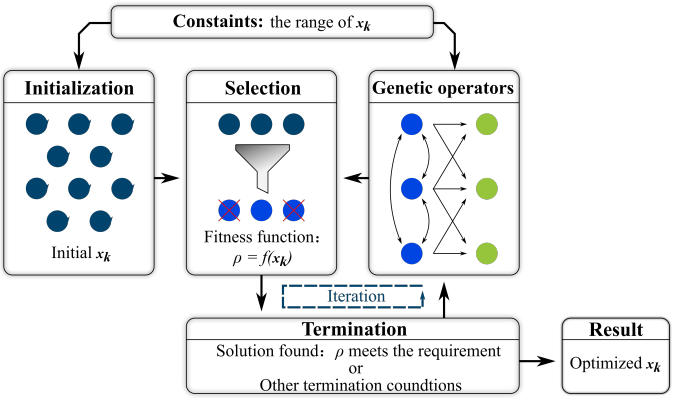

Fig. 6. Illustration of the proposed GA-based algorithm: the target is to select the x_k as the winding configuration for the homogeneous-flux transmitting coil.

Based on the design target and the flux-density model built in section II, each process is described in detailed:

- Initialization
  In the beginning, a group of candidates are generated, and the quantity of the candidates is named *population*. In the proposed algorithm, one candidate is a vector $\mathrm{x}_n = [x_1, x_2, ..., x_k]$ to representing a transmitting coil's winding configuration. The quantity of the population significantly impacts the consuming time for the final convergence. Typically, the initial candidates should be generated randomly to guarantee that a global optimized solution can be found.

- Selection
  In this procedure, the candidate is under evaluation. The process simulates the natural selection process. With this, a fitness function is introduced to quantify the evaluation. In the proposed algorithm, the fitness function defines the smoothness of the generated flux density as

$$\rho(h_p, r_p, k, \mathrm{x}_n) = \frac{Std.(\vec{\mathrm{B}_{q_1}}, \vec{\mathrm{B}_{q_2}}, ...\vec{\mathrm{B}_{qs_{kt}}})}{Avg.(\vec{\mathrm{B}_{q_1}}, \vec{\mathrm{B}_{q_2}}, ...\vec{\mathrm{B}_{q_{kt}}})} \times \begin{bmatrix} 0 \\ 0 \\ 1 \end{bmatrix} \quad (12)$$

  for the air-core transmitting coil or as

$$\rho(h_p, r_p, h_s, t_s, \mu_r, k, \mathrm{x}_n) = \frac{Std.(\vec{\mathrm{B}_{qs_1}}, \vec{\mathrm{B}_{qs_2}}, ...\vec{\mathrm{B}_{qs_{kt}}})}{Avg.(\vec{\mathrm{B}_{qs_1}}, \vec{\mathrm{B}_{qs_2}}, ...\vec{\mathrm{B}_{qs_{kt}}})} \times \begin{bmatrix} 0 \\ 0 \\ 1 \end{bmatrix} \quad (13)$$

  for the shielding transmitting coil. In equation (12) and (13), the h_p is the vertical distance between the transmitting and the receiving coils; r_p is the radius of the region where the flux is expected to be homogeneous. The fitness function is defined as the ratio between the standard deviation of the vertical flux density of the testing points and the average value of the vertical flux density. Besides, the smoothness can also be determined by the number of testing points (kt), increasing which a much homogeneous generated flux density can be obtained while more calculation resource is required. A lower fitness function value means a homogeneous distribution of magnetic flux being achieved by the transmitting coils, which is the optimization target for the algorithm.

- Genetic operators
  Genetic operators are to generate the next-generation candidates from the candidates passing the last selection. The candidates after the genetic operators are supposed to have better performance for evaluation.

- Termination
  The termination is a must for an iteration algorithm. In the proposed algorithm, three termination conditions are selected: 1. The value of the fitness function is lower than the threshold, meaning the target winding configuration has been found; 2. The difference of the fitness function between the two generations is lower than the threshold, meaning the best winding configuration has been found, though the target configuration may not be obtained under the constraints. The designer may modify the constraints, such as the number of windings or the shielded material's parameters to improve the flux density distribution; 3. The operational time is beyond acceptable: normally, the initial candidates' setting and the population's size should be modified to accelerate the algorithm.

- Constraints
  In the constraints, the features of candidates are limited during the entire iteration process. The most important constraint of the algorithm is the maximum value in the vector x_k to limit the geometry of the coils. Besides, the coil's practical implementation should be considered coils, such as the minimum value of the windings' radius and the pitch of the windings.

IV. Case Study for Design Demonstrations and Verifications

This section presents the detailed design process, design result analysis, and simulation/experiment verification for the proposed design algorithm based on two case studies

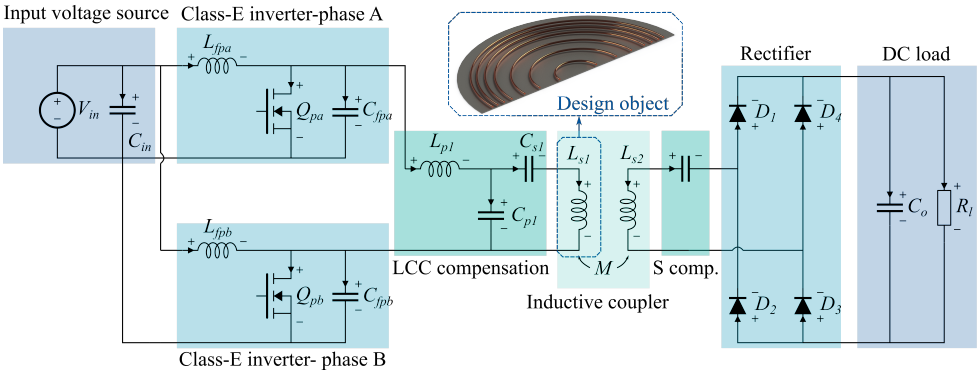

Fig. 7. The topology of the experimental prototype for the proposed design: the converter consists of a differential class-E inverter, an LCC-S compensated inductive coupler and a full-bridge rectifier. The DC-DC voltage-gain is designed as constant with a constant mutual inductance between the transmitting and receiving coils.

Table II
Key parameters of the inverter/ rectifier for the experimental prototype

Parameter	Value	Description
Q_{pa}, Q_{pb}	TP65H070LDG	Cascaded GaN MOSFET
$D_1 - D_4$	C3D10060A	SiC Schottky Diode
L_{fpa}/L_{fpb}	644 nH *	Air-core inductor
C_{fpa}/C_{fpb}	513 pF *	Equivalent capacitance

*The values are designed value.

for the air-core and the shielded transmitter coils. In Fig.7, the topology of the proof-of-concept IPT prototype is provided, which consists of a class-E inverter, the inductive coupler with LCC-S compensation and the full-bridge diode rectifier. As indicated in [24,25] , the class-E inverter and the full-bridge diode rectifier in the prototype achieve a constant voltage gain. The voltage gain of the LCC-S compensated coupler only depends on the value of mutual inductance M and the compensation inductance L_1. Thus, the improved position tolerance can be directly verified by the voltage gain from the DC output to the DC input for the IPT prototype. In table II, the parameters of the inverter and the rectifier are provided.

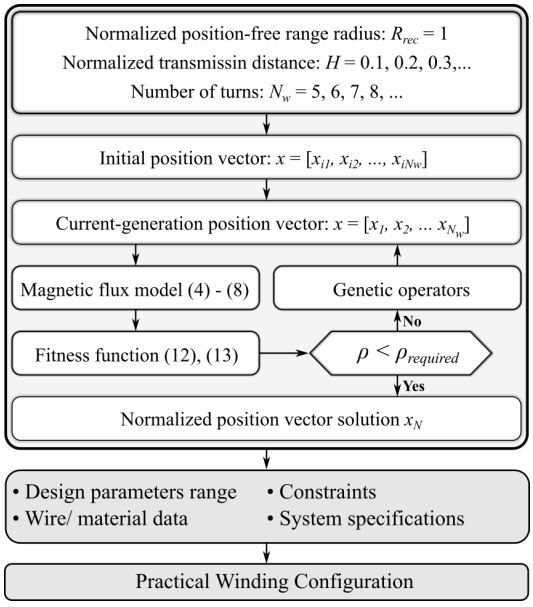

Fig. 8. Illustration of the proposed GA-based air-core homogeneous-flux transmitting coil design algorithm: the design can firstly be applied with normalized parameters, and the practical configuration can be obtained by size scaling.

A. Design Process and Experimental Verification for Air-Core transmitting Coils

For the air-core transmitter coils, with simplification where each turn of winding is regarded as filamentary current, a normalized solution can be given by an off-line design process, as shown in 6. The practical winding configuration can be obtained by the size scaling.

We provide the normalized design results by setting the radius of the position-free receiving range R_{rec} as 1 (in the SI base unit) and sweeping the transmission distance as 0.1/ 0.2/ 0.3 times of the receiving's range. The number of turns for the coils was also swept from 5 to 15 for different configurations. Several constraints in the design include: firstly, the searching range of position vector x should be limited to avoid the radius of the windings converging to a large value. Naturally, with elements in the vector x reaching large, meaning the radius of each winding's position is large as well, a homogeneous flux locating at the center of the coil can be obtained, but it is obviously not the desired solution for the transmitting coil design. The value range from 0.3 to 1.5 is recommended. For many cases the upper range can be further reduced to 1.3 to get the normalized solution. In addition, the termination condition can be applied that the difference of two successive fitness function is smaller than 0.5%, which

Table III
Optimization results for air-core transmitting coil regarding magnetic flux-density generated, average flux density and the flux's smoothness

	No. of turns(N_w)	5	6	7	8	9	10	11	12	13	14	15
0.1	$B_{avg}(\mu\mathrm{T})$	3.531	4.297	4.799	5.611	6.039	7.053	7.401	8.250	9.409	8.867	1.005
	$B_{avg}/N_w(\mu\mathrm{T})$	0.706	0.716	0.686	0.701	0.671	0.705	0.673	0.688	0.724	0.633	0.067
	ρ	0.112	0.083	0.063	0.057	0.053	0.042	0.040	0.034	0.024	0.034	0.024
0.2	$B_{avg}(\mu\mathrm{T})$	2.981	3.648	4.084	4.586	5.142	5.833	6.111	6.777	7.232	7.752	8.274
	$B_{avg}/N_w(\mu\mathrm{T})$	0.596	0.608	0.583	0.573	0.571	0.583	0.556	0.565	0.556	0.554	0.552
	ρ	0.052	0.036	0.032	0.027	0.021	0.017	0.016	0.01	0.012	0.01	0.09
0.3	$B_{avg}(\mu\mathrm{T})$	2.292	2.809	3.323	3.894	4.435	4.829	5.167	5.575	6.039	6.540	7.202
	$B_{avg}/N_w(\mu\mathrm{T})$	0.458	0.468	0.475	0.487	0.493	0.483	0.470	0.465	0.465	0.467	0.480
	ρ	0.041	0.032	0.022	0.015	0.011	0.010	0.009	0.008	0.006	0.005	0.004

means under the condition the best solution has been found. The primary target/termination condition should always be set as the fitness function reaches the target (in the design is set as 0.02%).

The results have been verified by three times optimization process to minimize the design uncertainty from the improper initial position vectors. However, it must be emphasized that the GA-based algorithm cannot guarantee that the results converge into the global optimized solution but to approach it. Besides, the results also depends on the parameter setting in the algorithm, mainly including the size of the population, the consumed computing power and the accepted computation consuming time. In Fig. 9, the magnetic flux density generated by the designed coil is plotted as the function of the position for transferred distance, set as 0.1, 0.2 and 0.3. TableIII presents the values of the average magnetic flux density within the receiving range for each case, the corresponding flux density generated per turn, and the converged fitness function. Due to the excitation current on each turn in the winding is set as 1 thus with the increasing of the number of turns, the intensity of the magnetic flux generated is also increased for a specific power transferring distance. Nevertheless, no pattern can be found regarding the generated flux density per turn due to the irregular distribution of the windings for each configuration. Besides, it can be noticed that a more homogeneous flux density can be generated with higher power transferring distance, and at the position out of the target receiving range, the flux density is reduced sharply. The direction of the flux turns even reversely for many cases. Generally in inductive power transfer systems, a higher generated flux density from the transmitting coil usually contributes to efficiency improvement. Thus, the designer must make a trade-off between the power transfer efficiency and the position tolerance of the inductive couplers.

We also implemented one air-core homogeneous-flux transmitting coil on the prototype to experimentally verify the design, whose winding configurations are listed in TableIV. The practical winding configurations are ob-

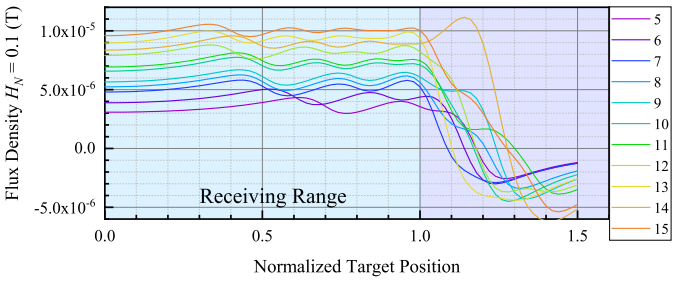

(a)

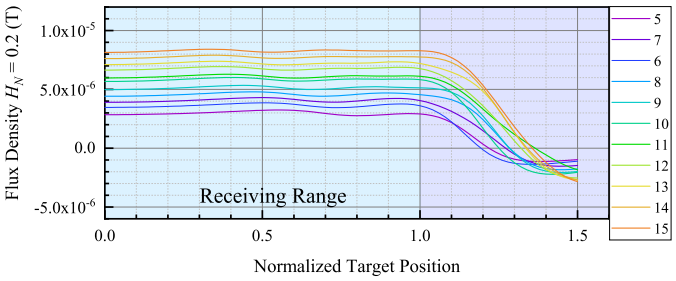

(b)

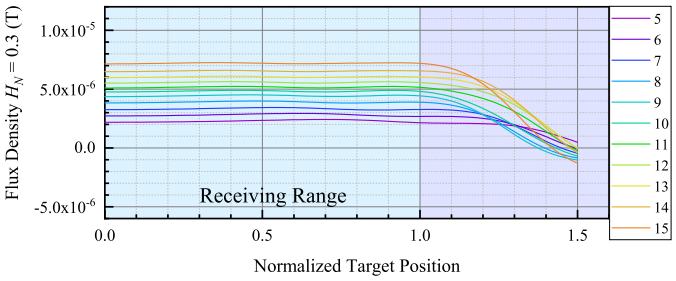

(c)

Fig. 9. The generated flux density of the design results is plotted as the function of the position to show the smoothness of the flux distribution: (a) The normalized power transfer distance equals to 0.1. (b) The normalized power transfer distance equals to 0.2. (c) The normalized power transfer distance equals to 0.3.

Table IV
Parameters of the air-core transmitting coil on the experimental prototype

transmitting coil	Normalized design input	Nw = 8 , HN = 0.2 , RN = 1
	Normalized winding configuration	radius = [0.59, 0.95, 1.12, 1.16, 1.21, 1.25, 1.30, 1.35]]
	Practical winding configuration	radius = [32.40, 52.30, 61.50, 64.00, 66.50, 69.00, 71.50, 74.15]mm mm
	Inductance(μH)	Modeled: 12.08, 2D-FEM: 11.46, Small-signal measurement: 12.41
receiving coil	Practical winding configuration	3 turns: radius = [25.00, 27.00, 29.00]mm
	Inductance(nH)	Modeled: 835.34, 2D-FEM: 868.61, Measurement: 909.85 *

Measurement was made by small-signal impedance analyzer 4294A.

Table V
Parameters of the shielded transmitting coil on the experimental prototype

transmitting coil	Design input Practical winding configuration Inductance(μH)	N_w = 8 , H_p = 15 mm , R_p = 50 mm radius = [34.00, 55.71, 60.74, 62.97, 66.00, 68.36, 72.30, 75.00] Modeled: 14.21, 2D-FEM: 14.56, Measurement: 15.75*
receiving coil	Practical winding configuration Inductance (nH)	3 turns: radius = [25.00, 27.00, 29.00] mm Modeled: 835.34, 2D-FEM: 868.61, Measurement: 909.85*
Magnetic Shielding	Magnetic material Parameters	EFF03 from KEMET h_s = 2 mm, T_s = 0.3 mm, μ_s = 128

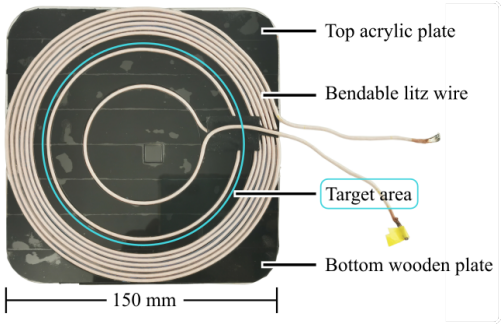

Fig. 10. The photo of the position-free air-core coil implemented on the prototype.

tained by using the outer radius of the winding (75 mm) scaled by the normalized solution and the power transfer distance is scaled as 11 mm. The self-inductance of the transmitting coils are modeled, simulated and measured by impedance analyzer as 12.08, 11.46 and 12.41 μH correspondingly. It validates the precision of the analytical model. The photo of the air-core coil is shown in Fig.9 (a). As shown the windings positions were limited by the transparent PMMA supporter, whose shapes were carved by the laser cutter; both the PMMA supporter and the winding are sustained on a wooden supporter.

The design concept and method for the air-core transmitting coils are verified by 2D FEM simulation as well as experimental results in Fig.9. In Fig.9 (a), the flux density generated by the air-core coil from the modelling and the 2D FEM simulation is plotted, which indicates a good matching from the modelling to the simulation results. By applying the modelling, the flux estimation can be simplified to reduce the effort for entity modelling and FEM simulation during the design, and also makes it possible to integrate it into advanced optimization algorithm. In addition, the experimental results of the prototype are given in Fig.9 (b) and (c): in Fig.9 (b), the operation for the transmitting-side is presented with the measured voltage waveforms on switches Q_{pa} and Q_{pb} and the measured current on the transmitting coil. The operation transmitter-side is almost not interfered with by the receiver coil's position shift, where the waveforms perform identical under the position shift, as shown in the figure. Moreover, Fig. 9 (c) plots the measured output voltage and power on the load, which reflects the output can be maintained constant during the position shift as well. When the receiving coil is placed out of the target position-free range, the output voltage/power will be reduced because the lower quantity of flux is coupled to transfer power to the load. All these observations validate that the proposed design achieved an improved position tolerance for the IPT system.

B. Design Process and Results Analysis for Shielded transmitting Coils

Unlike the homogeneous-flux solution with air-core transmitting coils, the design for the shielded coil cannot be obtained from scaling the normalized solutions because the space of the electromagnetic field is not homogeneous but distorted by the magnetic shielding materials. Thus, the design specifications for the power transfer should serve directly as the input of the design algorithm, as illustrated in Fig.12. We also implement the shielded homogeneous-flux transmitting on the prototype for experimental verification. The photo of the transmitting coil with the magnetic shielding is shown in Fig.13, where the magnetic sheet initially for EMI shielding was used. The detailed winding and shielding configurations can be

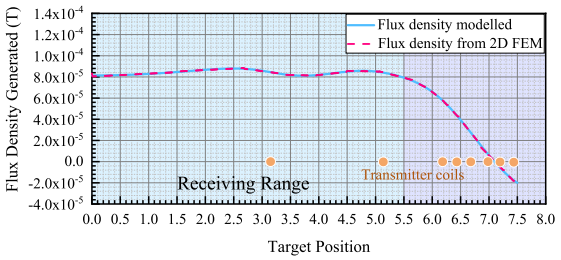

(a)

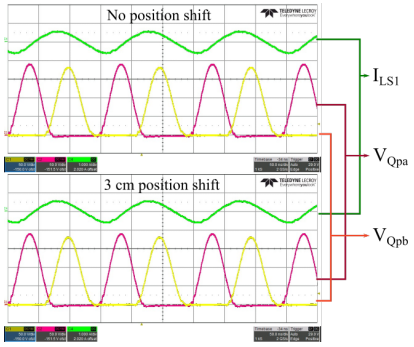

(b)

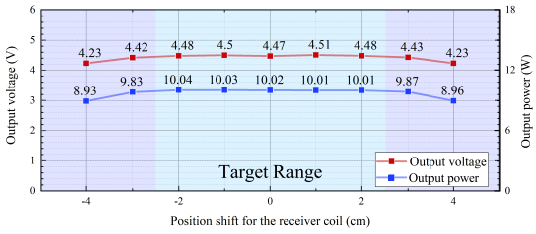

(c)

Fig. 11. Simulation and experimental verification for the design of air-core transmitting coil: (a) the calculated and 2D FEM simulated magnetic flux-density guaranteed based on the design are plot for the position of the receiving coil. A good matching can be observed to indicate the analytical model can estimate the coil's performance well. (b) The operation waveforms on the primary-side for the switches and the coils. Even with a receiving's position shift, the operation maintain relatively stable, which verify the position tolerance for the inverter. (c) The measured output voltage and power under position shift of the receiving coil. The output maintain constant to verify the enhanced position tolerance.

found in Table V. The design input directly generates the winding configuration for the shielded coil. The power transfer distance is set as 15 mm, and the radius of the position-free receiving set as 50 mm. In addition, the magnetic shielding material is implemented by the EFF03 EMI shielding from KEMET, whose thickness is 0.3 mm and the permeability is 128 at the operational frequency. Particularly, it needs to be mentioned that the modeled inductance and the 2D FEM simulated inductance for the coils match well with each other while the small-signal measured inductance is found higher. The difference may come from the measurement because it is difficult to verify that the proper magnetization is applied to the materials. The large-signal test is even harder to accomplish. Nevertheless, the modelling can give a rapid and relatively precise estimation of the inductance. The following measurement results indicate that it can also be integrated into the proposed design algorithm.

Similarly, the magnetic flux generated by the implemented shielded transmitting coil is verified by the FEM simulation. In Fig.14 (a), the excellent matching can be found as well. With applying the position-free shielded transmitting coil, the position shift was found not to interfere with the operation both for the inverter and the rectifier as well, as illustrated Fig.14 (b) and (c). Particularly as in the Fig.14 (c), a constant output voltage of 22 V and output power of 20 W can be achieved even with a 2 cm position shift for the receiving coil, which verifies a large position tolerance is achieved by the proposed design. A noticeable output reduction can be observed when the receiving coils move out of the target range, conforming to the flux distribution estimated by the modelling and the 2D FEM simulation results.

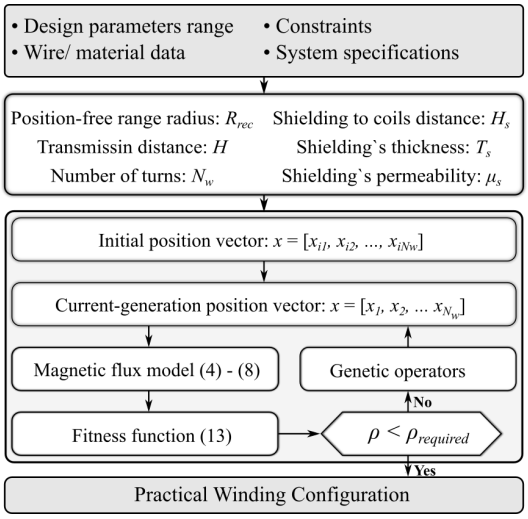

Fig. 12. Illustration of the proposed GA-based shielded homogeneous-flux transmitting coil design algorithm.

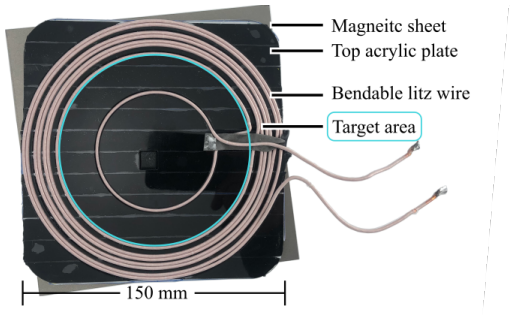

Fig. 13. The photo of the position-free shielded coil implemented on the prototype.

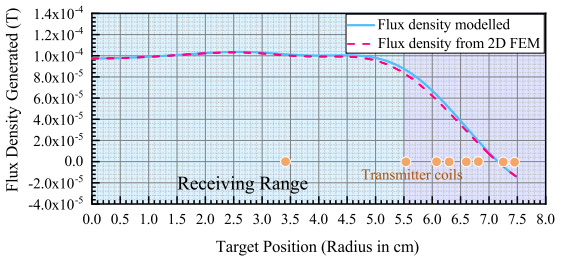

(a)

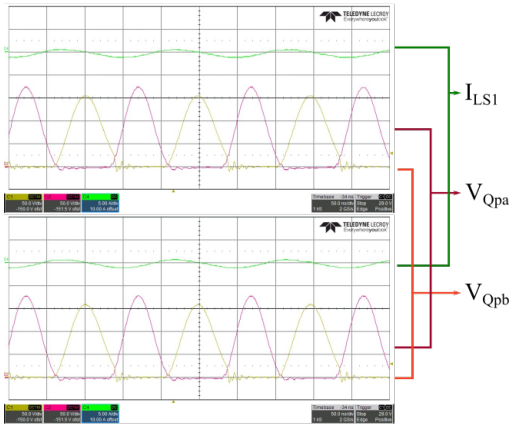

(b)

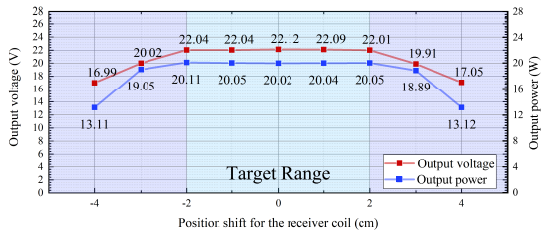

(c)

Fig. 14. Simulation and experimental verification for the design of air-core transmitting coil: (a) the calculated and 2D FEM simulated magnetic flux-density guaranteed based on the design are plot for the position of the receiving coil. A good matching can be observed to indicate the analytical model can estimate the coil's performance well. (b) The operation waveforms on the primary-side for the switches and the coils. Even with a receiving's position shift, the operation maintain relatively stable, which verify the position tolerance for the inverter. (c) The measured output voltage and power under position shift of the receiving coil. The output maintain constant to verify the enhanced position tolerance.

V. Conclusion

In this investigation, a design method that combines an analytical magnetic-flux model with the genetic algorithm (GA) is proposed to generate the position-free transmitter coil design in inductive power transfer systems, analyzed, and experimentally verified. The analytical models and design methods are proposed correspondingly for the air-core coil and shielded coil, extending the application range for the inductive power transfer. Based on the investigation, several key observations and conclusions are made:

(1) The position-free function can be achieved by the design concept that the constant magnetic flux is coupled by the receiving coil. The homogeneous-flux transmitting coil can accomplish the design concept. This concept contributes to a reliable and straightforward design for inductive power transfer applications, where a high position tolerance is usually desired.

(2) The presented analytical models can estimate the magnetic flux generated by air-core coils and shielded coils. The results can match well with the 2D FEM simulation results and measurement results. In particular, the mirror method can simplify the magnetic field solving for the shielded coils, thus avoiding the efforts during the FEM simulation.

(3) Combining the analytical model allows the winding configurations for the homogeneous transmitter coil to be directly generated, for both in air-core or shielded structure. The normalized design parameters can be scaled for practical air-core transmitter coil design to avoid algorithm implementation.

(4) The proposed design can be simulated and experimentally verified. A 6.78 MHz WPT system, where the proposed transmitter coil designs are implemented, performs an excellent position tolerance for the receivers' position shift. As a result, the inverter's operation and the output do not interfere with the position shift.

References

[1] S. Y. Hui, "Planar wireless charging technology for portable electronic products and qi," Proceedings of the IEEE, vol. 101, no. 6, pp. 1290–1301, 2013.

[2] S. Li and C. C. Mi, "Wireless power transfer for electric vehicle applications," IEEE Journal of Emerging and Selected Topics in Power Electronics, vol. 3, no. 1, pp. 4–17, 2015.

[3] G. A. Covic and J. T. Boys, "Modern trends in inductive power transfer for transportation applications," IEEE Journal of Emerging and Selected Topics in Power Electronics, vol. 1, no. 1, pp. 28–41, 2013.

[4] X. Li, C.-Y. Tsui, and W.-H. Ki, "A 13.56 mhz wireless power transfer system with reconfigurable resonant regulating rectifier and wireless power control for implantable medical devices," IEEE Journal of Solid-State Circuits, vol. 50, no. 4, pp. 978–989, 2015.

[5] S.-U. Shin, M. Choi, S. Jung, H.-M. Lee, and G.-H. Cho, "A time-interleaved resonant voltage mode wireless power receiver with delay-based tracking loops for implantable medical devices," IEEE Journal of Solid-State Circuits, vol. 55, no. 5, pp. 1374–1385, 2020.

[6] M. Sugino and T. Masamura, "The wireless power transfer systems using the class e push-pull inverter for industrial robots," in 2017 IEEE Wireless Power Transfer Conference (WPTC), 2017, pp. 1–3.

[7] M. R. Barzegaran, H. Zargarzadeh, and O. Mohammed, "Wireless power transfer for electric vehicle using an adaptive robot," IEEE Transactions on Magnetics, vol. 53, no. 6, pp. 1–4, 2017.

[8] X. Dai, J. Wu, J. Jiang, R. Gao, and U. K. Madawala, "An energy injection method to improve power transfer capability of bidirectional wpt system with multiple pickups," IEEE Transactions on Power Electronics, vol. 36, no. 5, pp. 5095–5107, 2021.

[9] F. Sangare, Y. Xiao, D. Niyato, and Z. Han, "Mobile charging in wireless-powered sensor networks: Optimal scheduling and experimental implementation," IEEE Transactions on Vehicular Technology, vol. 66, no. 8, pp. 7400–7410, 2017.
[10] W. X. Zhong, X. Liu, and S. Y. R. Hui, "A novel single-layer winding array and receiver coil structure for contactless battery charging systems with free-positioning and localized charging features," IEEE Transactions on Industrial Electronics, vol. 58, no. 9, pp. 4136–4144, 2011.
[11] Z. Dang and J. A. A. Qahouq, "Modeling and investigation of magnetic resonance coupled wireless power transfer system with lateral misalignment," in 2014 IEEE Applied Power Electronics Conference and Exposition - APEC 2014, 2014, pp. 1317–1322.
[12] R. Bosshard, U. Iruretagoyena, and J. W. Kolar, "Comprehensive evaluation of rectangular and double-d coil geometry for 50 kw/85 khz ipt system," IEEE Journal of Emerging and Selected Topics in Power Electronics, vol. 4, no. 4, pp. 1406–1415, 2016.
[13] X. Liu and S. Y. Hui, "Optimal design of a hybrid winding structure for planar contactless battery charging platform," IEEE Transactions on Power Electronics, vol. 23, no. 1, pp. 455–463, 2008.
[14] E. Waffenschmidt, "Homogeneous magnetic coupling for free positioning in an inductive wireless power system," IEEE Journal of Emerging and Selected Topics in Power Electronics, vol. 3, no. 1, pp. 226–233, 2015.
[15] J. R. Sampson, "Adaptation in natural and artificial systems (john h. holland)," 1976.
[16] X. Huang, W. Chen, and Q. Chen, "A design algorithm of circular transmitting coil to achieve uniform magnetic field distribution in wpt applications," in 2015 IEEE 2nd International Future Energy Electronics Conference (IFEEC), 2015, pp. 1–5.
[17] D. J. Griffiths, "Introduction to electrodynamics," 2005.
[18] E. Waffenschmidt, "Shielding properties of soft-magnetic layers for planar inductors," in Proceedings of 14th International Power Electronics and Motion Control Conference EPE-PEMC 2010, 2010, pp. S15–17–S15–24.
[19] J. Biela, "Optimierung des elektromagnetisch integrierten serien-parallel resonanzkonverters mit eingeprägtem ausgangsstrom," Ph.D. dissertation, ETH Zurich, 2005.
[20] W. G. Hurley and M. C. Duffy, "Calculation of self and mutual impedances in planar magnetic structures," IEEE Transactions on Magnetics, vol. 31, no. 4, pp. 2416–2422, 1995.
[21] E. Waffenschmidt, B. Ackermann, and J. A. Ferreira, "Design method and material technologies for passives in printed circuit board embedded circuits," IEEE Transactions on Power Electronics, vol. 20, no. 3, pp. 576–584, 2005.
[22] H. Cui, J. Mullenix, R. Massolini, and K. D. T. Ngo, "Field modeling for plate-core inductor with significant fringing using equal-flux contours," IEEE Transactions on Magnetics, vol. 53, no. 9, pp. 1–10, 2017.
[23] J. H. Holland et al., Adaptation in natural and artificial systems: an introductory analysis with applications to biology, control, and artificial intelligence. MIT press, 1992.
[24] X. Huang, Y. Dou, S. Lin, Y. Tian, Z. Ouyang, and M. A. E. Andersen, "Synchronous push–pull class e rectifiers with load-independent operation for megahertz wireless power transfer," IEEE Transactions on Power Electronics, vol. 36, no. 6, pp. 6351–6363, 2021.
[25] Y. Dou, X. Huang, Z. Ouyang, and M. A. Andersen, "Modelling and compensation design of class-e rectifier for near-resistive impedance in high-frequency power conversion," IEEE Transactions on Power Electronics, vol. 36, no. 8, pp. 8812–8823, 2021.